EES Batteries

PAPER

Composite Cathode Material for Improved Aluminum-Polymer Batteries†

Shuvrodev Biswas,*[a] Thomas Köhler, [a], Amir Mohammad,[a], Hartmut Stöcker,[a] and Dirk C. Meyer,[a]

[a] *Institute of Experimental Physics, TU Bergakademie Freiberg, Leipziger Str. 23, 09599 Freiberg, Germany; E-mail: shuvrodev.biswas@physik.tu-freiberg.de*

Supporting information

1 Experimental

1.1 Synthesis of the composites

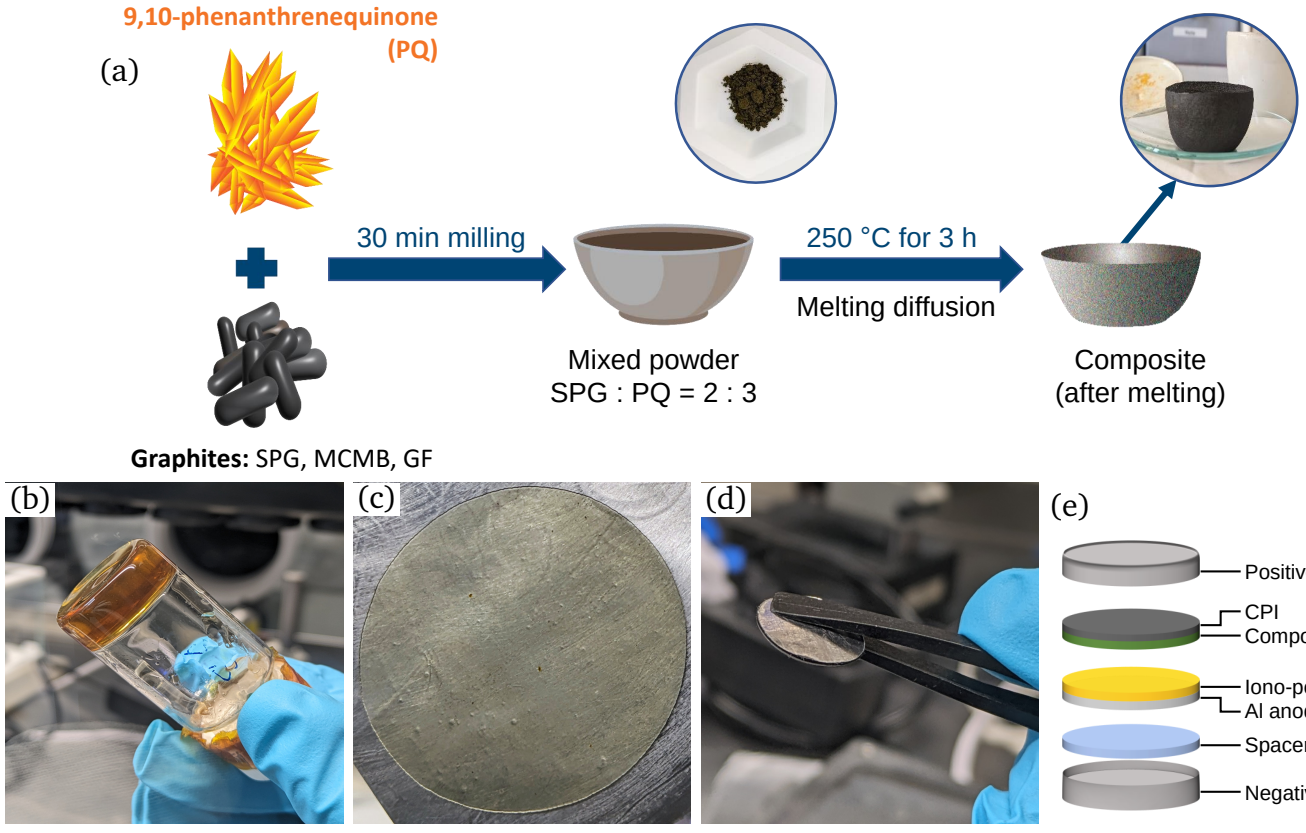

Fig. S1 Different steps of cathode synthesis and RAB construction: a) sketch of composite synthesis with the final mold of SPGPQ after thermal treatment, b) solid polymer electrolyte based on $AlCl_3$, Et_3NHCl and PA6, c) electrolyte applied on Al anode, d) a sandwich of electrodes and electrolyte, and e) schematic illustration of RAB components in a CR2016 case.

The composites were synthesized using a melt-diffusion process. For this, spherical graphite (SPG, 20 – 30 µm, 99 – 100 %, Sigma Aldrich) and 9,10-Phenanthrenequinone (PQ, 99.99 %, Sigma Aldrich) were milled (planetary ball mill Retsch P100) at a ratio of 2:3 for 30 min ensuring a uniformly mixed powder. The ratio was chosen based on an estimation from previous studies (for example, Yoo *et al.* [1]) to ensure optimal melt diffusion, minimizing the presence of either excess

uncoated graphite or surplus molten PQ without a host structure. The milling was done in a 50 ml ZrO_2 jar with 80 g of ZrO_2 balls (2 mm diameter) at 500 rpm for 30 min. The powder mixture was then heated for 3 h at $250\,^{\circ}\mathrm{C}$, i.e. $\approx 40\,^{\circ}\mathrm{C}$ higher than the melting temperature of PQ, in an Ar-filled container so that PQ melts and coats the SPG particles. After cooling down to room temperature, a mold of the composite (SPGPQ) was obtained, which was then crushed using a mortar for electrode slurry preparation. To analyze the influence of the graphite shape, two other forms of graphite, namely meso carbon micro-beads, (MCMB, $20\,\mu\mathrm{m}$, 99.94 %, TOB New Energy Technology) and synthetic graphite flakes, (GF, $< 20\,\mu\mathrm{m}$, 99.99 %, Sigma Aldrich) were used for the synthesis of similar composites following the same process and ratio. Figure S1 a presents the steps of composite synthesis at a glance.

1.2 Cathode preparation

The composite cathode slurry was prepared by mixing 80 wt.% of composite powders (SPGPQ, GFPQ, or MCMBPQ), 10 wt.% polymethyl methacrylate (PMMA, Alfa Aesar) as a binding additive, and 10 wt.% carbon black (CB, Alfa Aesar) as a conductive additive with a disperser (IKA T25 Ultra Turrax) for 50 min at 20000 rpm. At first, PMMA was completely dissolved in N-Methyl-2-pyrrolidone (NMP, 99 %, Sigma Aldrich) by magnetic stirring and the other powders were added slowly while dispersing. After the preparation of the slurry, it was coated on conductive polyimide foil (CPI, 60 $\Omega/\square \pm 10\,\%$, thickness $50\,\mu\mathrm{m}$, Ryan Technology & Co. Ltd.) using a doctor blade and dried for 10 h at $70\,^{\circ}\mathrm{C}$. The mass loading of active materials in the electrodes was varied from 2 to 5 mg/cm^2 with a dry coating thickness range of $40-60\,\mu\mathrm{m}$.

For performance comparisons, a similar procedure was carried out for other types of cathodes, for example, MCMB, SPG, and GF using the same ratios. In the case of pure PQ electrodes, the ratio of PQ, CB, and PMMA was changed to 70:20:10 considering the poor electrical conductivity of PQ.

1.3 Preparation of solid iono-polymer electrolyte (SPE)

The solid iono-polymer electrolyte consists of 99.999 % anhydrous aluminum chloride ($AlCl_3$, Alfa Aesar), triethylamine-hydrochloride (Et_3NHCl, 99.9 %, Sigma Aldrich), and polyamide-6 (PA6, > 98 %, $50\,\mu\mathrm{m}$, Sigma Aldrich) at a molar ratio of 2.8:1:1 following the process mentioned in our previous work[2]. In short, an ionic liquid of $AlCl_3$ and Et_3NHCl was prepared at a ratio of 2:1 and heated to $80\,^{\circ}\mathrm{C}$ for 3 h to assist the solid-solid reaction. After that, the rest of the $AlCl_3$ and PA6 were added and heated for 3 h at $100\,^{\circ}\mathrm{C}$ for the completion of the polymerization reaction. Finally, a transparent brown iono-polymer electrolyte is obtained (see Figure S1 b), where the ratio of $AlCl_3$ and (Et_3NHCl + PA6) is 1.4 (2.8/2).

1.4 Construction of RABs

All of the cathodes were used for cell preparation. For this purpose, at first iono-polymer electrolyte (thickness $200\,\mu\mathrm{m}$) was applied on the Al anode (thickness $30\,\mu\mathrm{m}$, Carl Roth) using a heated pressing tool inside a glovebox with an inert atmosphere (see Figure S1 c). A sandwich of electrodes and electrolyte was then obtained by placing the cathode on top of the pressed electrolyte (see Figure S1 d). The cathode and anode each have an area of 2 cm^2. A commercial CR2016 cell housing was used for encapsulating the sandwich along with stainless steel spacers. Figure S1 e shows a schematic of a coin cell with its components.

1.5 Electrochemical study

The resistance (R) of the cathodes with CPI was measured using a Keithley 2400 Source-measure unit at a constant current of 10 mA with a 4-wire setup. The conductivity was then calculated using $\sigma = \frac{t}{\pi r^2 R}$, where t is the thickness of the electrode and r is the radius (6 mm)[3,4].

For all the electrochemical measurements, BioLogic SP-50 and BCS-805 devices were used. In this case, cyclic voltammetry and galvanostatic cycling with potential limitation (GCPL) were carried out at room temperature. Temperature-controlled cycling was conducted inside an oven using a custom holder to understand the temperature impact on the cell performance. In every case of GCPL, the voltage windows for the composite, pure PQ and graphites were 2.35 V – 0.5 V, 1.8 V – 0.2 V and 2.35 V – 0.8 V, respectively. A complete list of the cathodes used in this study along with their respective purposes are given in Table S1.

1.6 X-ray diffraction

The investigations of the changes in the crystal structure of pristine SPG, PQ and SPGPQ composite were carried out using X-ray diffraction analysis. For this, a Bruker D8 Advance diffractometer with Cu anode (λ = 1.5406 Å) was used at 40 kV and 40 mA. The diffraction pattern was recorded over a 2θ range of 5° to 70° with a step size of $\Delta 2\theta = 0.01^\circ$ and Δt = 1 s. For this, samples were mounted on a polymer holder. A fixed illumination slit (20 mm) was used on the primary side while a soller slit limiting the axial divergence to 2.5° and a Lynxeye XE-T 1D detector in high-resolution mode were positioned on the secondary side.

To confirm the intercalation of $AlCl_4^-$ during charging and deintercalation during discharging, *operando* XRD analysis of an Al cell with composite cathode and an Al cell with SPG cathode were carried out. In this case, a Bruker D8 Discover with a Cu anode (λ = 1.5406 Å) was used at 40 kV and 40 mA. On the primary side, a Goebel mirror, a vertical slit of 0.6 mm and a horizontal slit of 10×2 mm, and on the secondary side, a Lynxeye 1D detector were used for recording the diffraction pattern while cycling the cells. Both cells were charged and discharged at 85 mA/g using a BioLogic SP-50 potentiostat. For both of the cells, CR2016 coin cell cases with a conductive polyimide window on the cathode side were used. The diffraction patterns were recorded for a 2θ range of 5° to 60° at $\Delta 2\theta = 0.05^\circ$ and $\Delta t = 0.5$ s.

1.7 Fourier transform infrared (FT-IR) spectroscopy

The stability and reaction mechanism of the cathodes were investigated by attenuated total reflectance (ATR) in the infrared region. Full cells were made from an aluminum anode, iono-polymer electrolyte, and SPGPQ composite cathode. The cells were charged (at 90 mA/g), discharged (at 70 mA/g), or kept in electrolyte contact, whereby the cathode was free of residues of the polymer electrolyte. The two electrochemical states (charged and discharged) were compared with an as-prepared cathode. For the stability investigation and comparison with pure PQ cathodes, both SPGPQ and PQ cathodes were kept in contact with the electrolyte for 5 min and 30 min. The ATR FT-IR spectra of the cathodes were then recorded with a Bruker Tensor 37 and a Bruker Platinum ATR unit in the range of 400–$3000\,\mathrm{cm}^{-1}$ at a resolution of $2\,\mathrm{cm}^{-1}$ (apodised) with a beam diameter of 3.5 mm. A Blackman-Harris 3-term function was used for apodisation. Since the cathode slurry was produced with carbon black, germanium served as the ATR crystal. The samples were mounted in the Ar glovebox, using a special ATR press plunger for air-sensitive samples. The cathode side, which was in contact with the electrolyte, was always pressed onto the Ge crystal with the same pressure. The press-on plunger applied the necessary pressure to confirm full-surface contact with the reflective element and at the same time seal the sample from the surrounding atmosphere and avoid possible side reactions with air. The resulting ATR spectra were represented as absorption spectra using the equation ATR = absorption coefficient $\times\, \nu$/1000, where ν is the wavenumber. As the penetration depth in ATR measurements is inversely proportional to the wavenumber, the spectra were normalized to a constant penetration depth using the Bruker OPUS software[5,6].

1.8 X-ray photoelectron spectroscopy

XPS is an effective tool for investigating the electroactive species. *Ex-situ* XPS was performed to determine the active species contributing to charging and discharging. For this, a Thermo Fisher Escalab 250Xi spectrometer was used to record the data, where a monochromatic Al-$K\alpha$ X-ray tube (E = 1486.6 eV) was used as the source, with an excitation angle to the surface normal of 45°. A hemispherical analyzer with 6 channeltrons is used, mounted in the direction of the surface normal. Three different samples: pristine cathode, charged cathode (at 50 mA/g until 2.35 V), and discharged cathode (at 50 mAh/g until 0.5 V) were examined. In order to analyze the samples subjected to electrochemical treatment, the RABs were disassembled within a glovebox. Subsequently, the cathodes were meticulously transferred into the XPS chamber utilizing a custom vacuum holder to ensure the integrity of the specimens. All measurements were performed at room temperature and the data was analyzed using CasaXPS software.

1.9 Electromagnetic spin resonance (ESR) spectroscopy

Investigations of electrodes using ESR spectroscopy are of interest due to the change in the magnetic state of the atoms caused by the transformation of the crystal structure or the incorporation/removal of charge carriers such as metal cations or electrons. ESR spectroscopy is a convenient tool for elucidating the intercalation mechanism that takes place and its reversibility[7,8]. To conduct ESR measurements on the cathodes, they were carefully disassembled in an inert argon atmosphere to prevent oxidation. The active electrode material was gently removed from the current collector by scratching.

The material was subsequently transferred into a sealed glass tube to protect it from atmosphere exposure. The sample mass was also carefully recorded to normalize the data. ESR spectra were acquired immediately using a MS5000 ESR spectrometer (Freiberg Instruments) at X-band frequency (9.46 GHz) under the following conditions: microwave power of 15 mW, amplitude modulation of 0.5 mT, sweep time of 400 seconds and 15 accumulations. All measurements were performed at room temperature and the data was analyzed using ESR studio from Bruker.

1.10 Electrode properties

For different purposes, multiple cells with varying parameters were used. The specific capacity and specific energy density are calculated based on the mass of the active material. The Coulombic efficiency is written as the average CE $\pm$ standard deviation. Table S1 presents cathode properties and their corresponding usage in electrochemical analysis, including details on various active materials, such as thickness, total mass, active material mass loading, current density, and specific purpose.

Table S1 Cathode properties and their corresponding usage in electrochemical analysis

Purpose	**Active material**	**Cathode mass (mg)**	**Active material mass loading (mg/cm^2)**	**Thickness** (μm)	**Charge current density (mA/g)**	**Discharge current density (mA/g)**
operando XRD	SPG	5.0	2.0	47	85	85
	SPGPQ	5.0	2.0	45	85	85
FT-IR	PQ	6.0	2.4	47	90	–
	SPGPQ	7.0	2.8	52	–	70
ESR	SPGPQ	7.0	2.8	48	70	–
	SPGPQ	7.0	2.8	50	–	70
XPS	SPGPQ	7.0	2.8	50	50	–
	SPGPQ	7.2	2.9	55	–	50
Temperature controlled	SPGPQ	5.0	2.0	52	225	225
Cyclability	SPGPQ	6.3	2.5	52	25	25
	GFPQ	6.3	2.5	52	25	25
	MCMBPQ	7.5	3.0	52	25	25
	PQ	4.0	2	45	25	25
	SPG	11.0	4.4	60	25	25
	SPGPQ (wet)	5.0	2.0	52	25	25
	PQ (wet)	6.0	2.4	45	25	25
	SPG (wet)	11.0	4.4	62	25	25
	SPGPQ	6.0	2.5	52	210	175
	SPGPQ	6.0	2.5	52	150	150
	MCMBPQ	5.0	2.0	52	150	150
	GFPQ	5.0	2.0	52	150	150

2 Spectroscopic data

The XPS and EDX measurements were performed for surface elemental analysis of the pristine, charged and discharged sample. Figure S2 presents the XPS survey spectra, pristine C 1s and O 1s. The detailed elemental analysis is discussed in section 3.3.3 of the main article.

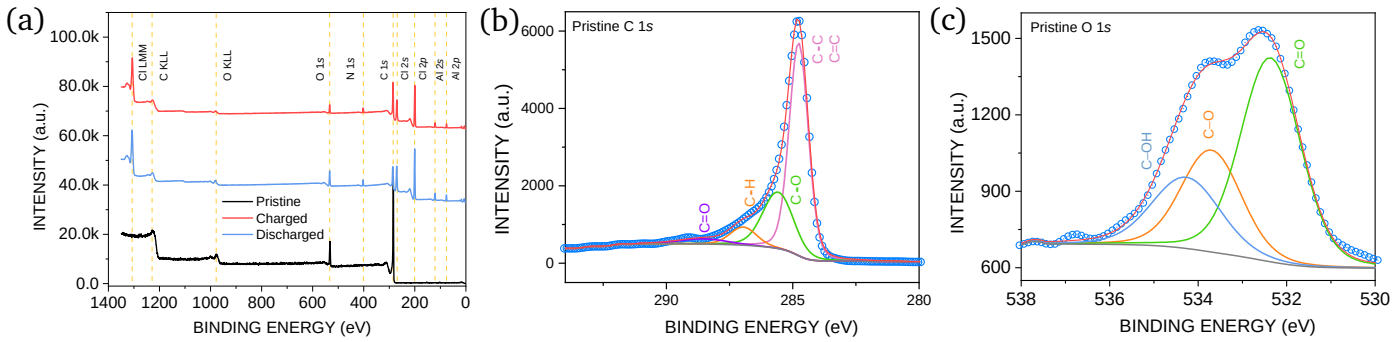

Fig. S2 Spectroscopic data: a) survey spectra of pristine, charged and discharged cathodes, elemental spectrum of pristine cathode: b) C 1s and c) O 1s.

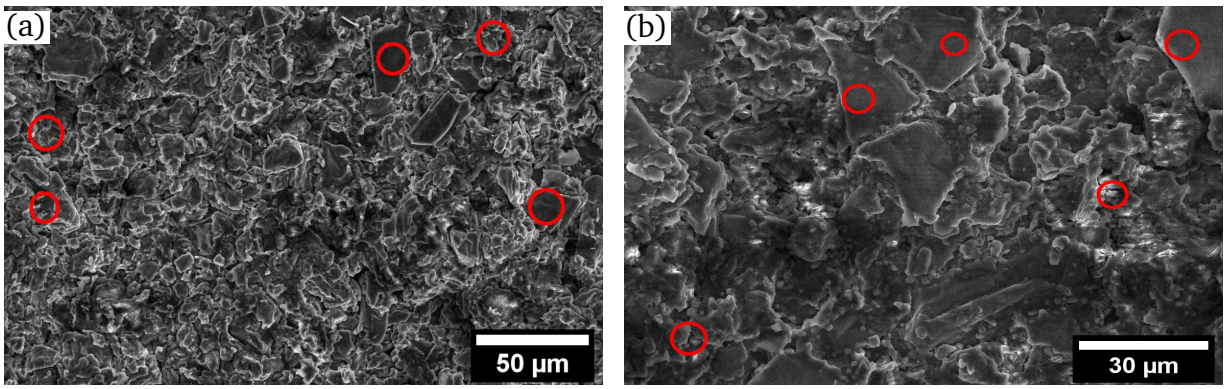

Fig. S3 Scanned points of EDX analysis: a) fully charged cathode and b) fully discharged cathode.

The elemental concentrations were determined using X-ray photoelectron spectroscopy (XPS) and energy dispersive X-ray spectroscopy (EDS). The results including the Al and Cl ratio are shown in Table S2. For EDS, point analysis was conducted on charged and discharged cathodes at multiple spots (see Figure S3 a and b) using 5 kV acceleration voltage and an Apollo XL-SDD EDAX detector.

Table S2 Concentration of C, O, Al and Cl of charged and discharged cathodes

	Element	**XPS** (At %)	**EDX** (At %) average ± SE
Charged	C	48.9	31.2 ± 12.8
	O	6.2	5.2 ± 2.8
	Al	10.0	12.9 ± 2.4
	Cl	39.9	52.7 ± 13.8
	Cl/Al	4.0	3.8 ± 0.4*
Discharged	C	62.9	66.7 ± 6.5
	O	4.0	12.8 ± 5.4
	Al	12.3	8.6 ± 2.2
	Cl	27.3	11.9 ± 2.5
	Cl/Al	2.2	2.0 ± 0.6*

* The average ratio (EDX) is calculated from individual ratios at multiple points as this approach provides a more representative value than the individual measurements.

3 Electrochemical Studies

3.1 Calculation of the theoretical capacities

The theoretical capacity of a material can be calculated using the following equation[9,10]:

$$C_{\text{theoretical}} = \frac{n \cdot F}{n_{\text{atom}} \cdot M_{\text{element}}}$$

where: n = number of electrons exchanged, F = 2.68×10^4 mAh/mol (Faraday constant), M_{element} = molecular mass of the element in g/mol and n_{atom} = number of atoms involved.

To calculate the theoretical capacity of graphite, we consider stage-4 intercalation, as indicated by *operando* XRD analysis. Since each graphite unit cell contains two graphene layers, two unit cells contribute to the intercalation. According to density functional theory (DFT) calculations by Pan et al.[10], four $AlCl_4^-$ ions intercalate into every fourth layer of graphene, where each layer consists of a 4×4 supercell. With 4 C atoms per unit cell, for 4 ions of $AlCl_4^-$, $2 \times 4 \times 4 \times 4$ carbon atoms are utilized. In other words, for each $AlCl_4^-$ ion, $128/4 = 32$ carbon atoms are engaged.
Thus the theoretical capacity of graphite (M = 12 g/mol) is:

$$C_{\text{SPG(theoretical)}} = \frac{1 \cdot 2.68 \times 10^4 \text{ mAh/mol}}{32 \cdot 12 \text{ g/mol}} = 69.8 \text{ mAh/g}$$

The theoretical capacity of PQ (M = 208 g/mol) is:

$$C_{\text{PQ(theoretical)}} = \frac{1 \cdot 2.68 \times 10^4 \text{ mAh/mol}}{1 \cdot 208 \text{ g/mol}} = 128.8 \text{ mAh/g} \quad (AlCl_2^+, \text{ 1 electron process})$$

$$C_{\text{PQ(theoretical)}} = \frac{2 \cdot 2.68 \times 10^4 \text{ mAh/mol}}{1 \cdot 208 \text{ g/mol}} = 257.7 \text{ mAh/g} \quad (AlCl^{2+}, \text{ 2 electrons process})$$

In the investigated composite the mass ratio of PQ and SPGPQ is 3:2. The molar masses of the SPG and PQ are 384 g/mol and 208 g/mol. Therefore, the molar ratio in the composite of PQ and SPG is 3/208:2/384 or 2.77:1.

3.2 Fitting parameters

The composite has a synergistic influence of its components which is distinctively observed in their voltage-capacity profile. A linear combination is used to evaluate their individual contributions, as described in the Battery performance section

of the main text. Here, Table S3 presents the calculated fractional contribution of PQ (x) and performance enhancement factor (y) along with their associated fitting errors.

Table S3 Fitting parameters for composite with 95 % confidence interval

Condition	Fractional contribution of PQ (x)	Performance enhancement factor (y)
Charge (SPE)	0.565 ± 0.003	1.750 ± 0.003
Discharge (SPE)	0.755 ± 0.019	1.586 ± 0.014
Average (SPE)	0.660 ± 0.011	1.668 ± 0.009
Charge (wet cathode)	0.390 ± 0.010	1.565 ± 0.024
Discharge (wet cathode)	0.663 ± 0.004	1.439 ± 0.004
Average (wet cathode)	0.526 ± 0.007	1.502 ± 0.014

3.3 Comparison of cathodes

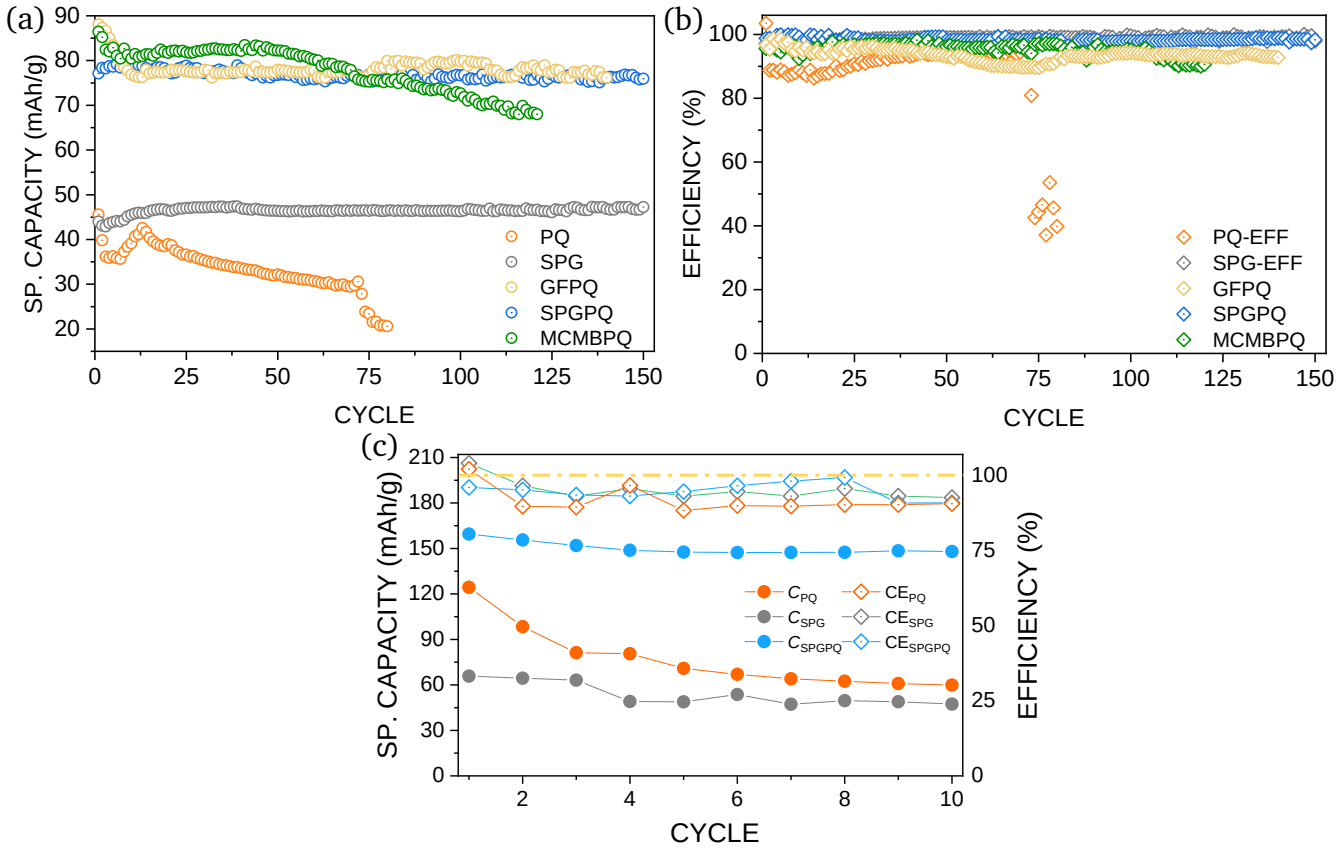

Fig. S4 Cyclability comparison between composites and their components: a) specific capacity and b) Coulombic efficiency without cathode wetting, c) with cathode wetting by IL.

Figure S4 presents a performance comparison of composites and their components without cathode wetting (see Figure S4 a and b). Figure S4 c) illustrates the cyclability of wetted cathodes. In all cases, cells were charged and discharged at 25 mA/g. The pure PQ cathode exhibits faster dissolution and capacity degradation when it is wetted using IL. In both cases, the composite offers improved performance in terms of capacity and stability. However, the CE lower than 90 % in

wet cathodes (see Figure S4 c) indicates the presence of side reactions that may compromise long-term cyclability.

References

1 D.-J. Yoo and J. W. Choi, *The Journal of Physical Chemistry Letters*, 2020, **11**, 2384–2392.

2 A. Mohammad, T. Köhler, S. Biswas, H. Stöcker and D. C. Meyer, *ACS Applied Energy Materials*, 2023, **6**, 2914–2923.

3 J. Entwistle, R. Ge, K. Pardikar, R. Smith and D. Cumming, *Renewable and Sustainable Energy Reviews*, 2022, **166**, 112624.

4 N. Mainusch, T. Christ, T. Siedenburg, T. ODonnell, M. Lutansieto, P. Brand, G. Papenburg, N. Harms, B. Temel, G. Garnweitner and W. Viöl, *Energy Technology*, 2016, **4**, 1550–1557.

5 Bruker Optics GmbH:, *OPUS Spectroscopic Software Reference Manual Version 5*, 2004.

6 T. Köhler, J. Hanzig and V. Koroteev, *Physical Sciences Reviews*, 2018, **4**, 20170154.

7 A. Vyalikh, T. Köhler, T. Zakharchenko, D. M. Itkis, A. Krajnc and G. Mali, *Physical Sciences Reviews*, 2018, **3**, 20170155.

8 A. Vyalikh, V. O. Koroteev, W. Münchgesang, T. Köhler, C. Röder, E. Brendler, A. V. Okotrub, L. G. Bulusheva and D. C. Meyer, *ACS Applied Materials & Interfaces*, 2019, **11**, 9291–9300.

9 J. Bitenc, N. Lindahl, A. Vizintin, M. E. Abdelhamid, R. Dominko and P. Johansson, *Energy Storage Materials*, 2020, **24**, 379–383.

10 C.-J. Pan, C. Yuan, G. Zhu, Q. Zhang, C.-J. Huang, M.-C. Lin, M. Angell, B.-J. Hwang, P. Kaghazchi and H. Dai, *Proceedings of the National Academy of Sciences*, 2018, **115**, 5670–5675.